

## Research Article

# Time Effect of Chloride Erosion on Physical and Mechanical Properties of High-Water-Content Materials

Hai-kuan Wu <sup>1,2</sup>, Chang-wu Liu <sup>1,2</sup>, Zhao Zhang<sup>1,2</sup> and Yi-chen Miao<sup>3</sup>

<sup>1</sup>State Key Laboratory of Hydraulics and Mountain River Engineering, Sichuan University, No. 24 South Section 1, Yihuan Road, Chengdu 610065, China

<sup>2</sup>College of Water Resource and Hydropower, Sichuan University, No. 24 South Section 1, Yihuan Road, Chengdu 610065, China

<sup>3</sup>Institute of Disaster Management and Reconstruction, Sichuan University—The Hong Kong Polytechnic University, No. 1 Huanghe Road, Chengdu 610065, China

Correspondence should be addressed to Chang-wu Liu; [liuchangwu@scu.edu.cn](mailto:liuchangwu@scu.edu.cn)

Received 8 January 2020; Revised 4 March 2020; Accepted 9 April 2020; Published 23 April 2020

Academic Editor: Veronica Calado

Copyright © 2020 Hai-kuan Wu et al. This is an open access article distributed under the Creative Commons Attribution License, which permits unrestricted use, distribution, and reproduction in any medium, provided the original work is properly cited.

In order to study the characteristics of high water-content materials (HWC) undergoing chloride erosion, we analyzed and summarized changes in strength, elastic modulus, and mass of HWC materials during chloride erosion using specific experimental research, and we also described the compression failure morphologies of HWC materials after erosion. The cuboid specimens developed a horizontal crack between the top and bottom, and the cylindrical specimens developed irregular encryption cracks at the top during increasing pressure. The erosion of HWC materials exposed to calcium chloride ( $\text{CaCl}_2$ ) solutions was relatively serious, and the erosion of the cuboid specimens was lower than that of the cylindrical specimens. The strength of HWC materials increased during prolonged erosion, and the strength of the cylindrical specimens in water was the highest, followed by the  $\text{CaCl}_2$  and sodium chloride (NaCl) solutions. However, the strength change of the cuboid specimens after 28 d was contrary to the above order. In late erosion stages, the HWC materials had better compactness and experienced smaller compressive deformation in water than the other two solutions. In the NaCl solution, the high-water filling material had more pores and a larger deformation than the other solutions.

## 1. Introduction

In China, HWC materials are mainly used to fill the goafs of coal mines. They can support the surrounding rock and restrict its deformation during the filling process, which cannot be separated from the excellent performance of HWC materials. At present, research into HWC materials has mainly concentrated on their application of underground engineering, the study of their basic mechanical properties, and the study of different admixtures involving them. Sun et al. [1] studied the influence of fly ash content on setting time, suspension, strength, and hydration heat release of HWC materials under different water-solid ratios. Sun et al. [2] analyzed the characteristics of displacement and stress with time in three stages of instantaneous, stable, and accelerated creep process of filling material with high-

water content. Liu et al. [3] have studied the law of surface subsidence and deformation after filling the goaf with HWC material. Guangming et al. [4] analyzed and studied the hydration mechanism and physical-mechanical properties of the HWC material and their role in water plugging by grouting. Wenying [5] studied the rheological properties of high-water filling paste. Mingkai et al. [6] studied the influencing factors of the properties of HWC materials. Song and Gao [7] studied the mechanism of grouting water shutoff in aquifers with organic HWC material grout. Xie and Chen [8] studied the creep behaviour of HWC materials under high pressure water environment. Li and Liu [9] studied the mechanical properties and damage constitutive model of HWC materials under different loading rates. Wang et al. [10] studied the surface subsidence control during mine filling with ultra-HWC materials in the Handan mining area.

However, underground projects are often inevitably affected by groundwater erosion. Groundwater chloride concentrations are often very high, which can have serious impacts on the structure of the project. Many experts have studied the effects of erosion on concrete [11–16]. Anitha et al. [17] studied the effect of corrosion inhibitors with ecological additives on the corrosion of reinforced concrete. Jain and Pradhan [18] studied the effects of chloride ions on the hydration, microstructure, and thermogravimetric properties of self-compacting concrete with different types of cement. Jee and Pradhan [19] carried out an experimental study on the relationship between durability parameters of concrete with different binders and chloride concentrations. Wang et al. [20] studied the water absorption and chloride diffusion of concrete under the coupling action of uniaxial compressive loads and freeze-thaw cycles. Zhang et al. [21] studied the water mass characteristics and corrosion potential of a mixed zone in a city's drinking water distribution system.

HWC materials are similar to concrete, which is also inevitably affected by erosion, but there are few reports about the effects of erosion on HWC materials. Therefore, in order to supplement the research on HWC materials, it is necessary to study the effects of erosion on them. In summary, this work has used this as justification to study the influence of chloride salts in groundwater on HWC materials.

## 2. Materials and Methods

**2.1. Materials.** According to the guidelines published by the China Standards Press (MT/T 420-1995), HWC materials (also known as high-water quick-setting materials) are a type of hydraulic material, consisting of two kinds of raw materials. The first raw material was material A and material A-A. Material A was made of bauxite, gypsum, etc., and was composed of composite super retarder and dispersant. The second material was composed of the B and B-B materials. The B material was made by mixing and grinding together gypsum and lime with a small amount of composite retarder. The ratio of the four components of HWC materials (A, A-A, B, and B-B) was 1 : 0.1 : 1 : 0.04, according to the proportion of various materials. The water-solid ratio was unchanged at 3 : 1. The A, A-A, B, and B-B materials were mixed with water according to the water solid ratio to form a slurry. The hydration hardening reaction occurred, and the final slurry was condensed to form a high water quick-setting material.

Materials A, A-A, B, and B-B were scanned with X-ray diffraction (XRD), and the results are shown in Figures 1–4. The main components of material A were  $3\text{CaO} \cdot 3\text{Al}_2\text{O}_3 \cdot \text{CaSO}_4$ , and  $2\text{CaO} \cdot \text{SiO}_2$ . The crystallinity of  $3\text{CaO} \cdot 3\text{Al}_2\text{O}_3 \cdot \text{CaSO}_4$  was better, as shown by the peak sharpness. The main components of material A-A were  $\text{Na}_2\text{CO}_3 \cdot \text{H}_2\text{O}$ ,  $\text{SiO}_2$ , and  $\text{NaHCO}_3$ . From the sharpness of the peak, the crystallinity of  $\text{Na}_2\text{CO}_3 \cdot \text{H}_2\text{O}$  and  $\text{SiO}_2$  was better and the crystallinity of  $\text{NaHCO}_3$  was worse. The main components of material B were  $\text{CaSO}_4$ ,  $\text{CaCO}_3$ , and  $\text{CaMg}(\text{CO}_3)_2$ . From the sharpness of the peak, the crystallinity of  $\text{CaSO}_4$  was the best and that of  $\text{CaMg}(\text{CO}_3)_2$  was poor. The main components of material B-B were  $\text{SiO}_2$  and  $\text{CaSO}_4$ . The crystallinity of  $\text{SiO}_2$  was the best, according to the sharpness of the peak [22].

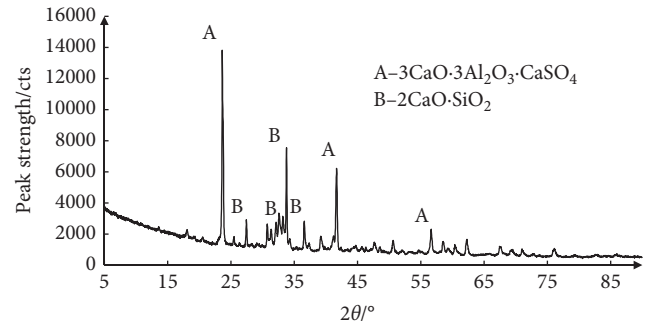


FIGURE 1: XRD of material A

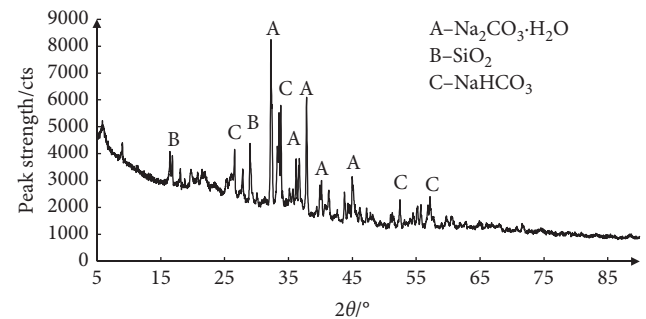


FIGURE 2: XRD of material A-A

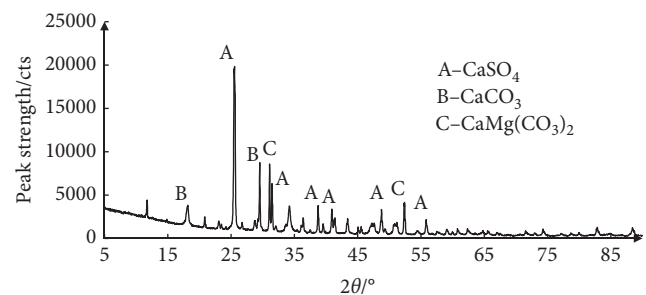


FIGURE 3: XRD of material B.

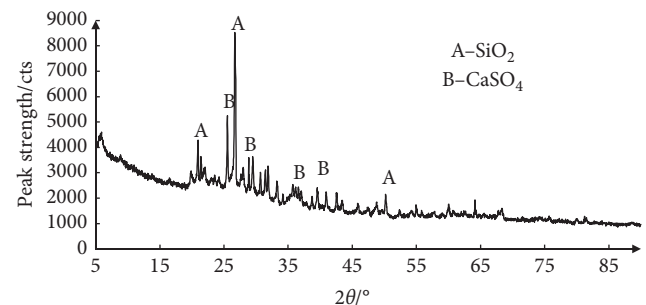


FIGURE 4: XRD of material B-B.

In engineering practice, there is a certain demand for different shapes of the same material. Different shapes lead to different materials properties in the same erosional environment, so it is necessary to study the properties of different

shapes of the same material exposed to chloride erosion. The specimens of HWC materials prepared in this experiment included cylindrical and cuboid specimens. The height of the cylindrical specimens was 100 mm, the diameter was 50 mm, and the surface area was  $35,325 \text{ mm}^2$ . The length and width of the cuboid specimens were 40 mm, the height was 160 mm, and the surface area was  $28,800 \text{ mm}^2$ . The poured specimens are shown in Figure 5. The erosion solution used in this experiment was composed of anhydrous NaCl and  $\text{CaCl}_2$ , with a mass fraction of 5%. The main mass indexes of the internal components are listed in Tables 1 and 2.



FIGURE 5: Specimen for pouring.

**2.2. Methods.** The HWC materials were prepared using a water-solid ratio of 3 : 1. A mixture of materials A and A-A were mixed with water, B and B-B were mixed with water, and then the two mixtures were combined to form the final HWC materials. The final mixtures were stirred evenly, and the specimens were poured into the mold and condensed for 2 h before demolding. Finally, the specimens were maintained in tap water for 7 d. The specimen prepared flow chart is shown in Figure 6:

In order to obtain the failure mode of the HWC material and understand the change in physical-mechanical properties with erosion time, uniaxial compression tests and mass measurements were carried out for one group specimen after curing for 7 d. During the loading process, the specimen was fixed in the middle of the instrument chassis before its size parameters were input into the computer. At the same time, the loading parameters were set to 3 mm/min, and the loading was started. The rest of specimens were soaked in solutions of NaCl,  $\text{CaCl}_2$ , and water, respectively. The strength, mass, and elastic moduli of the specimens during 7, 14, 21, and 28 d of soaking were tested. Strength and mass measurements were made of three specimens in the same batch. The strength measuring instrument used was a universal testing machine with a maximum load of 1 t. The specific parameters of the machine are shown in Table 3. An electronic balance was used in the mass measuring instrument. The test temperature was  $20 \pm 2^\circ\text{C}$ .

### 3. Results and Discussion

After the above tests, the following test results were obtained, including fracture morphology, mass, strength, and elastic modulus, which are discussed separately below.

**3.1. Fracture Morphology.** Figure 7 shows the compressive failure pattern of the cuboid specimen. When the pressure was increased gradually from zero, a penetrating crack was gradually formed from top to bottom. As the pressure increased, bulges and cracks occurred on the specimen sides, and it developed irregular horizontal cracks. When the pressure was increased further to its peak value, irregular columnar cracking occurred in the specimen.

Figure 8 shows the compressive failure pattern of the cylindrical specimen. When the pressure was increased gradually from zero, the specimen gradually formed a through-crack from top to bottom. As the pressure

TABLE 1: Mass indicators for internal components of anhydrous NaCl.

Chemical formula	Mass content (%)	Chemical formula	Mass content (%)
NaCl	$\geq 99.5$	$\text{PO}_4$	$\leq 0.001$
Water insoluble substance	$\leq 0.005$	N	$\leq 0.001$
$\text{SO}_4$	$\leq 0.002$	Ca	$\leq 0.005$
Fe	$\leq 0.0002$	Ba	$\leq 0.001$
Pb	$\leq 0.0005$	K	$\leq 0.02$
I	$\leq 0.002$	Mg	$\leq 0.002$
As	$\leq 0.00005$	Br	$\leq 0.01$
$\text{Fe}(\text{CN})_6$	$\leq 0.0001$		

TABLE 2: Mass indicators for internal components of anhydrous  $\text{CaCl}_2$ .

Chemical formula	Mass content (%)	Chemical formula	Mass content
$\text{CaCl}_2$	$\geq 96.0$	$\text{PO}_4$	$\leq 0.003\%$
Insoluble substance	$\leq 0.015$	N	$\leq 0.005\%$
$\text{SO}_4$	$\leq 0.020$	$\text{Ca}(\text{OH})_2$	$\leq 0.020\%$
Fe	$\leq 0.001$	Ba	Qualified
Pb	$\leq 0.001$	$\text{NO}_3$	Qualified
As	$\leq 0.0003$	Zn	$\leq 0.01\%$

continued to increase, the top cracks increased and became increasingly dense. When the pressure reached its peak value, the specimen was destroyed from the crack, and its shape was an irregular columnar block.

Comparing the fracture morphologies of the cuboid and cylindrical specimens, it was found that the cuboid specimen developed a horizontal crack in the process of producing longitudinal through-cracks, due to its long length. Moreover, during the fracture process, the cuboid specimen had a horizontal fracture between the top and bottom. The cylindrical specimen only underwent longitudinal irregular block fractures. The results showed that the fracture process of specimens with different shapes was significantly different.

**3.2. Mass.** Figure 9 shows the mass change of the cylindrical specimen of HWC materials soaked in  $\text{CaCl}_2$ , NaCl, and

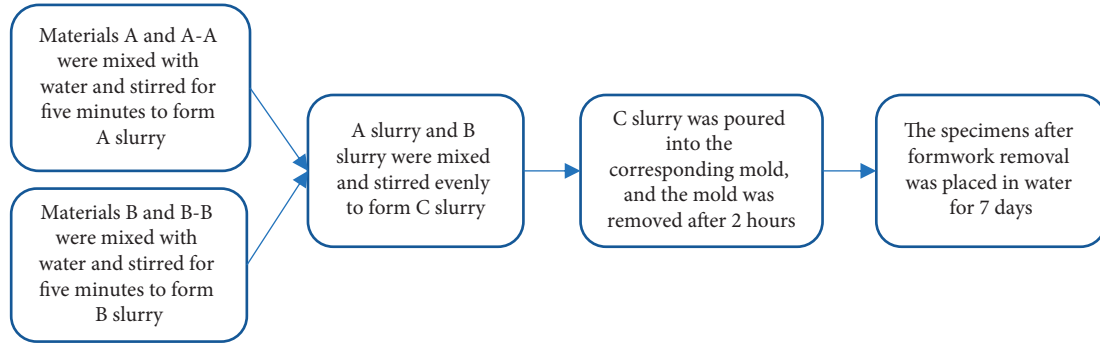


FIGURE 6: The specimen prepared flow chart.

TABLE 3: Parameters of the ETM-C electronic universal testing machine.

Parameters	Value
Model	ETM104B
Power supply	220V $\pm$ 10%
Host weight	400 kg
Outline size	775 * 660 * 1740 (mm)
Maximum test force	10 KN
Level of testing machine	One-level
Test force measurement range	0.2%~100%FS
Relative error of test force value	$\leq \pm 1\%$
Displacement resolution	0.065 $\mu$ m
Test force resolution	1/500000FS
Relative error of displacement value of crossbeam	$\leq \pm 0.5\%$
Adjustment range of crossbeam speed	0.001~500 mm/min
Relative error of crossbeam speed	$\leq \pm 1\%$ of set value
Width of effective test	420 mm
Maximum travel of crossbeam	1100 mm

water for 7, 14, 21, and 28d. The horizontal coordinate axis at 0 d represents the HWC materials that were cured in tap water for 7 d at  $20 \pm 2^\circ\text{C}$  and were uncorroded by other solutions. The coordinate axes in the other drawings have the same meaning. It was found that the mass of HWC materials increased rapidly from 0–7 d in  $\text{CaCl}_2$  solution but increased more slowly in the later 14, 21, and 28 d of erosion. The HWC materials in  $\text{NaCl}$  solution showed the same trend as in  $\text{CaCl}_2$  solution, but the increasing rate between 0–7 d was clearly slower than in  $\text{CaCl}_2$  solution. The mass change of HWC materials in tap water tended to be gentle, and the range of change was very small. Finally, the variation in the mass of the cylindrical specimen of HWC materials with erosion time in different solutions was predicted. By comparing with the experimental results, the predicted law had high reliability. Its predictive formulas are shown in the following:

$$M(\text{CaCl}_2) = -0.0147t^2 + 0.5994t + 260.06, R^2 = 0.8999, \quad (1)$$

$$M(\text{NaCl}) = -0.0086t^2 + 0.3337t + 255.16, R^2 = 0.856, \quad (2)$$

$$M(\text{H}_2\text{O}) = -0.0157t + 260.26, R^2 = 0.7035. \quad (3)$$

where  $M$  denotes mass and  $t$  denotes time, (d).

Figure 10 shows the mass changes of the cuboid specimen of HWC materials soaked in  $\text{CaCl}_2$ ,  $\text{NaCl}$ , and water for 7, 14, 21, and 28 d. The mass change of the cuboid specimen of HWC materials in solution over time was similar to that of the cylindrical specimen. In  $\text{CaCl}_2$  and  $\text{NaCl}$  solutions, the growth rate of the cuboid specimen in the  $\text{CaCl}_2$  solution was higher than that in the  $\text{NaCl}$  solution. Finally, the law of mass change with erosion time of the cuboid specimen of HWC materials in different solutions was predicted. By comparing with the experimental results, the predicted curve had high reliability. The corresponding predictive formulas were obtained and are shown as follows:

$$M(\text{CaCl}_2) = -0.0194t^2 + 0.7614t + 318.92, R^2 = 0.8584, \quad (4)$$

$$M(\text{NaCl}) = -0.0106t^2 + 0.4051t + 326.76, R^2 = 0.9375, \quad (5)$$

$$M(\text{H}_2\text{O}) = -0.0371t + 321.14, R^2 = 0.8579. \quad (6)$$

Figures 11 and 12 show the mass changes of specimens with different shapes in the same solution of HWC materials. In the  $\text{NaCl}$  solution, the mass of the cylindrical and cuboid specimens increased smoothly with time. The mass trends of the cuboid and cylindrical specimens were predicted. By comparing with the experimental results, the predicted law was reliable. The predictive formulas are as follows:

$$M(\text{Cuboid}) = 0.1071t + 327.8, R^2 = 0.5591, \quad (7)$$

$$M(\text{Cylindrical}) = 0.0929t + 256, R^2 = 0.5389. \quad (8)$$

In the  $\text{CaCl}_2$  solution, the mass of the cylindrical and cuboid specimens increased slowly over time in a small range. The predictive formulas are shown in the following:

$$M(\text{Cuboid}) = 0.2186t + 320.82, R^2 = 0.5575, \quad (9)$$

$$M(\text{Cylindrical}) = 0.1871t + 261.5, R^2 = 0.6317. \quad (10)$$

Figure 13 shows the mass changes of cylindrical and cuboid specimens of HWC materials in  $\text{NaCl}$  and  $\text{CaCl}_2$  solutions. The calculation formula is shown as follows:

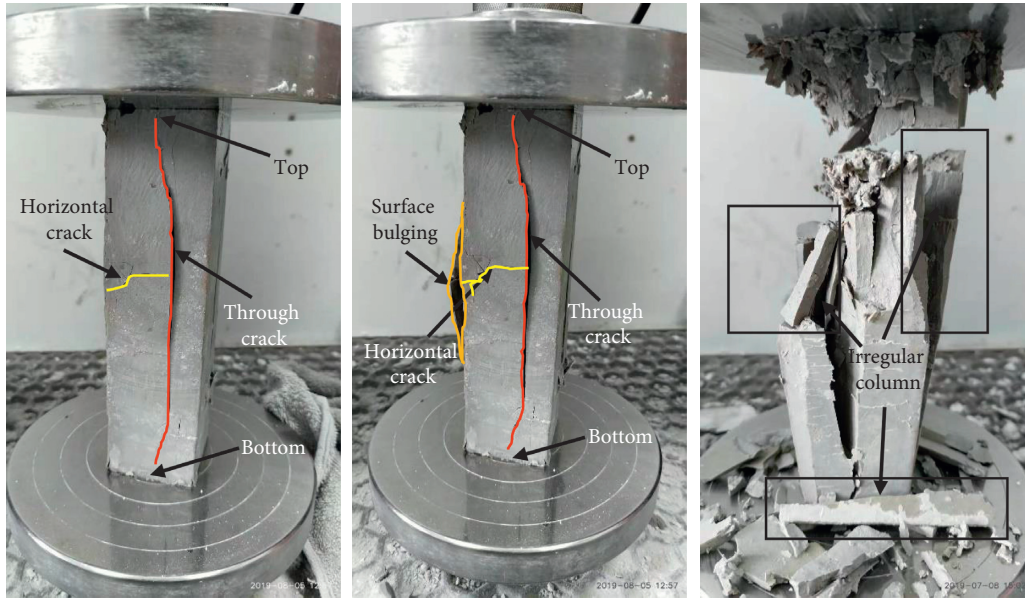


FIGURE 7: Fracture morphology of the cuboid specimen under compression.



FIGURE 8: Fracture morphology of the cylindrical specimen under compression.

$$R(m) = \frac{(m_1 - m_0)}{m_0}, \quad (11)$$

where  $R(m)$  represents the mass change,  $m_1$  represents the mass after erosion, and  $m_0$  represents the initial mass after 7 d of curing.

In the NaCl solution, the mass of the cylindrical specimen decreased from 0.0122 to 0.0118 g and then increased to 0.0126 g and the final mass increased by 0.0004 g. The mass of the cuboid specimen increased from 0.0095 to 0.0116 g and then decreased to 0.0107 g. The final mass increase was 0.0012 g. In the CaCl<sub>2</sub> solution, the mass of the cylindrical specimen increased from 0.0204 to 0.0239 g, and

the final mass increased by 0.0035 g. The mass of the cuboid specimen decreased from 0.0223 to 0.0217 g and then increased to 0.0236 g and the final mass increased by 0.0013 g. In generally, the final mass change of the cylindrical specimen was larger than that of the cuboid specimen because the surface area of the cylindrical specimen was larger than that of the cuboid specimen, the corrosion channels of the solution increased, and the corrosion speed was faster than that of the cuboid specimen. At the same time, due to the replacement reaction of sodium ions and calcium ions in solution and the internal composition of HWC materials, the products produced would be soluble in water. From the point of view of mass change, it can be seen that the erosion

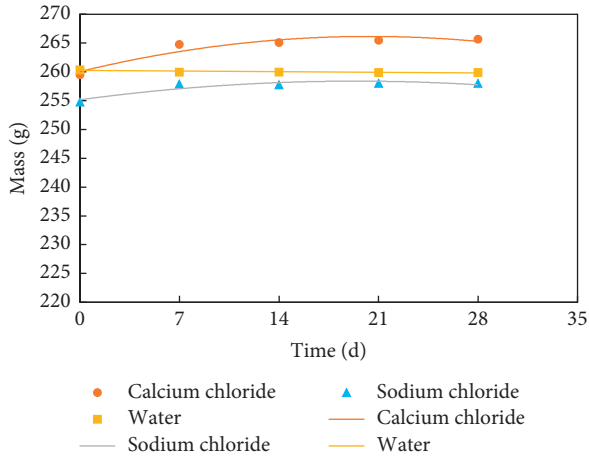


FIGURE 9: Mass change of the cylindrical specimen of HWC materials in different solutions.

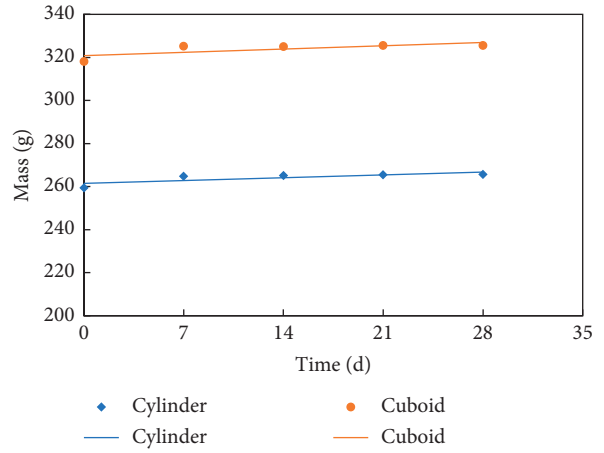


FIGURE 12: Mass changes of specimen with different shapes after erosion of CaCl<sub>2</sub> solution of HWC materials.

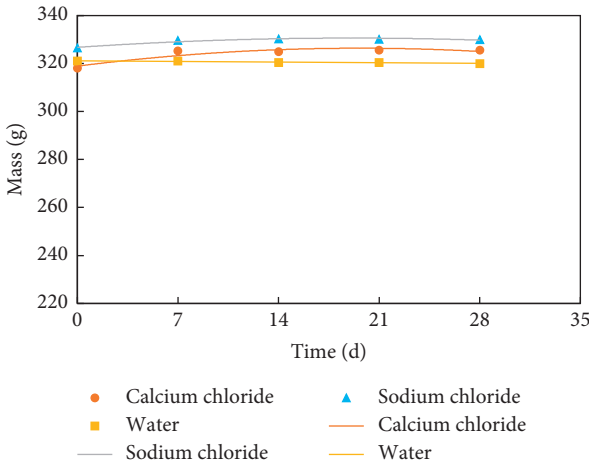


FIGURE 10: Mass change of the cuboid specimen of HWC materials in different solutions.

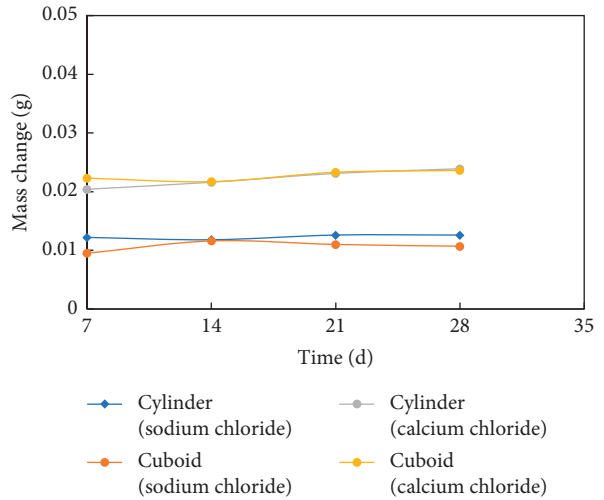


FIGURE 13: Mass change of HWC materials eroded by solution.

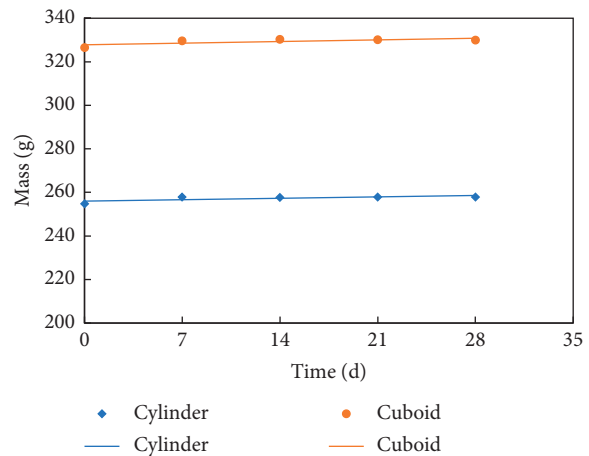


FIGURE 11: Mass changes of specimen with different shapes after erosion of NaCl solution of HWC materials.

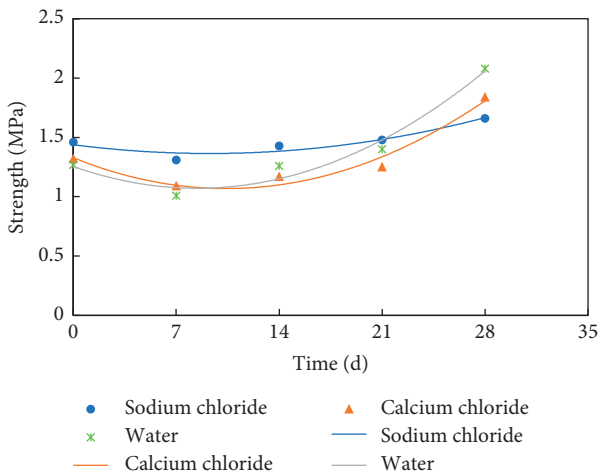


FIGURE 14: Peak compressive strength of the cylindrical specimen of HWC materials after erosion in different solutions.

of HWC materials in CaCl<sub>2</sub> solution was greater than that in NaCl solution, and the erosion of the cylindrical specimen was more serious than that of the cuboid specimen.

**3.3. Peak Strength.** Figure 14 shows the peak strength of the uniaxial compression test of a cylindrical specimen of HWC materials eroded in NaCl solution, CaCl<sub>2</sub> solution, and water. In the three solutions, the strength of the specimen first decreased and then gradually increased. The strength change of the specimen was the largest in water, followed by CaCl<sub>2</sub> solution, and the smallest change occurred in NaCl solution. Finally, the strength change trend was predicted in different solutions. By comparing with the experimental results, the reliability of the predicted curve was very well. The predictive curve formulas are as follows:

$$\sigma(\text{NaCl}) = 0.0009t^2 - 0.0159t + 1.4383, R^2 = 0.9035, \quad (12)$$

$$\sigma(\text{CaCl}_2) = 0.0024t^2 - 0.0498t + 1.3283, R^2 = 0.9611, \quad (13)$$

$$\sigma(\text{H}_2\text{O}) = 0.0026t^2 - 0.0435t + 1.2549, R^2 = 0.9645. \quad (14)$$

Figure 15 shows the strength change rate of the cylindrical specimen of HWC materials after erosion. The strength change formula is shown as follows:

$$R(\sigma) = \frac{(\sigma_1 - \sigma_0)}{\sigma_0}, \quad (15)$$

where  $R(\sigma)$  represents the change rate of strength,  $\sigma_1$  represents the strength after erosion, and  $\sigma_0$  represents the initial strength after 7 d of maintenance.

In the three solutions, the specimen strength eventually increased, but the range of increase was different. The increase in strength of the specimen cured in water was the largest, indicating that the strength of the specimen was still in an increasing stage, while the increase in the strength of the specimen in NaCl solution and CaCl<sub>2</sub> solution was significantly lower than that in water. The results showed that the specimen was affected to varying degrees by two corrosive solutions. Finally, the strength change in the CaCl<sub>2</sub> solution reached 0.3939 MPa, which was significantly higher than that in the NaCl solution. This was due to the fact that the CaCl<sub>2</sub> solution was more likely to form water-insoluble crystals in the specimen during the diffusion of the two chlorides, eventually leading to a strength increase greater than that in NaCl solution. Ettringite and calcium silicate hydrate play major roles in the strength of HWC materials [22, 23]. From the experimental results, we can see that in the early stage, the HWC materials in NaCl and CaCl<sub>2</sub> solutions produced the ability of ettringite and calcium silicate hydrate to be stronger than those in water. However, in the later stage, they showed better performance in water. Therefore, the erosion of chloride on HWC materials would be increasing seriously with the passage of time.

Figure 16 shows a comparison of the peak compressive strengths of the cylindrical and cuboid HWC material specimens after 28 d of erosion in the three solutions. Through data analysis, it was found that the strength of the cylindrical specimen and cuboid specimen had the same change trend, in the order of

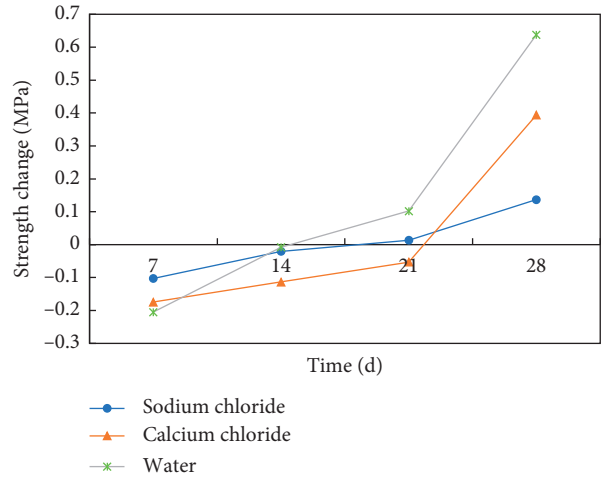


FIGURE 15: Strength change rate of the cylindrical specimen of HWC materials after erosion.

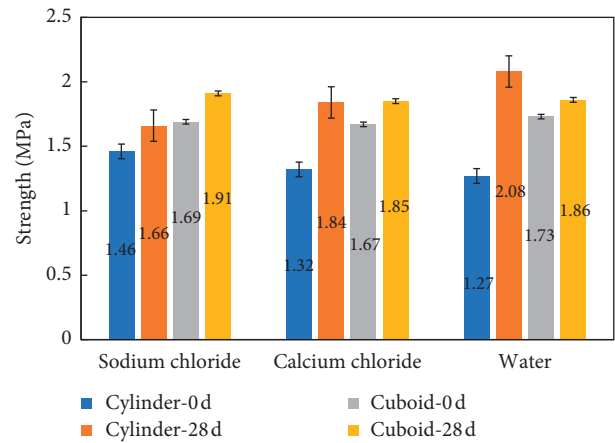


FIGURE 16: Strength of different specimens after 28 d of erosion by different solutions.

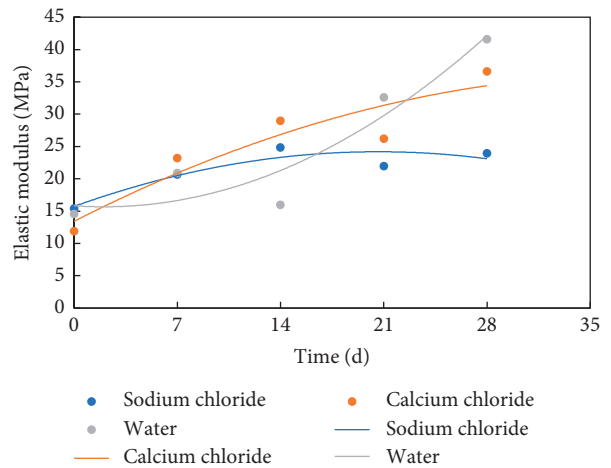


FIGURE 17: Change of elastic modulus of the cylindrical specimen with HWC materials.

water >CaCl<sub>2</sub> solution >NaCl solution. However, because the surface area of the cylindrical specimen was smaller than the cuboid specimen, the erosion rate of the cuboid specimen was faster than the cylindrical specimen, so the strength of the cuboid specimen increased less than that of the cylindrical specimen.

**3.4. Elastic Modulus.** Figure 17 shows the change in the elastic modulus of the cylindrical HWC materials specimen in three solutions. The overall trend was an increase, but the elastic modulus of the specimen increased more slowly in NaCl solution and more rapidly in water. In the CaCl<sub>2</sub> solution, there was a flat period in the middle. Both the initial and final stages increased, but the growth rate at the end stage was lower than that in water. We found that the HWC materials were compact in water and had little deformation in the later stage of erosion, while in NaCl solution, they had large deformations and pores. Finally, the trend of the elastic modulus change was predicted. By comparing with the experimental results, the predicted curve had high reliability. The predictive formulas are shown in the following:

$$E(\text{NaCl}) = -0.0199t^2 + 0.821t + 15.721, R^2 = 0.8528, \quad (16)$$

$$E(\text{CaCl}_2) = -0.015t^2 + 1.1701t + 13.407, R^2 = 0.8664, \quad (17)$$

$$E(\text{H}_2\text{O}) = 0.0392t^2 - 0.1594t + 15.83, R^2 = 0.8957. \quad (18)$$

## 4. Conclusions

From the analysis of fracture morphologies, changes in mass, compressive strength, and modulus of elasticity of HWC materials after erosion in chloride salt solutions, the following conclusions can be drawn:

- (1) From the fracture morphologies, it is clear that there is a significant difference between the fractures developed in the cuboid specimen and the cylindrical specimen. The cuboid specimen produced a horizontal crack between the top and bottom. While the cylindrical specimen developed irregular encryption cracks at the top as the pressure was increased.
- (2) From the point of view of mass, the erosion of HWC materials in CaCl<sub>2</sub> solution is relatively serious, and the erosion of the cuboid specimen was lower than that of the cylindrical specimen.
- (3) In terms of view of compressive strength, we show that the strength of HWC materials increases in the later stage of erosion. We found that the strength of the cylindrical specimen in water was the highest, followed by the CaCl<sub>2</sub> solution and the smallest in NaCl solution, while that of the cuboid specimen changed after 28 d.
- (4) From the point of view of elastic modulus, we reveal that HWC materials have good compactness in water and undergo small compression deformations in the later stage of erosion. In the NaCl solution, there were many small pores and deformation.

## Data Availability

The data used during the study are available from the corresponding author upon request.

## Conflicts of Interest

The authors declare that there are no conflicts of interest regarding the publication of this article.

## Acknowledgments

The authors thank the experimental platform provided by the Hydropower College of Sichuan University.

## References

- [1] D. S. Sun, H. U. Mei-Mei, A. G. Wang, K. W. Liu, and Y. M. Guan, "Research and preparation of high water filling material with high dosage of fly ash," *Bulletin of the Chinese Ceramic Society*, vol. 35, no. 4, pp. 1074–1079, 2016.
- [2] C. Sun, D. Zhang, X. Wang, and R. Zhou, "Large-size test on creep characteristics of high water material for filling body beside roadway," *Journal of Mining & Safety Engineering*, vol. 29, no. 4, pp. 1673–3363, 2012.
- [3] H. Liu, C. He, Z. Dong, Z. Niu, and Z. Zhang, "Surface subsidence based on filling technology with materials of high water content coal," *Geology & Exploration*, vol. 38, no. 6, pp. 54–61, 2010.
- [4] F. Guangming, H. Chaojiong, and H. Yongnian, "Special material for blocking against water by grouting in pit shaft engineering," *Coal Technology of Northeast China*, vol. 6, pp. 22–24, 1998.
- [5] L. Wenyong, "Study on rheological behavior of high-water rapid-setting material slurry China safety," *Science Journal*, vol. 4, pp. 28–31, 1997.
- [6] Z. Mingkai, Z. Wensheng, and L. Beixing, "Properties of rapid setting and solidifying material with high water content and investigation on its hardening mechanism," *Journal of Wuhan University of Technology*, vol. 4, pp. 18–21, 1998.
- [7] Y.-B. Song and Q.-C. Gao, "Mechanism of grouting for waterproof using organic material with high water content," *Journal of Mining & Safety Engineering*, vol. 3, pp. 320–323, 2006.
- [8] H. Xie and Y. Chen, *Experimental Research on Creep Laws of High-Water Material under Real Pressure Water Environment*, *Key Engineering Materials*, pp. 350–354, Trans Tech Publications, Stafa-Zurich, Switzerland, 2016.
- [9] X. Li and C. Liu, "Mechanical properties and damage constitutive model of high water material at different loading rates," *Advanced Engineering Materials*, vol. 20, no. 6, 2018.
- [10] X. Wang, D. Zhang, C. Sun, and Y. Wang, "Surface subsidence control during bag filling mining of super high-water content material in the Handan mining area," *International Journal of Oil, Gas and Coal Technology*, vol. 13, no. 1, pp. 87–102, 2016.
- [11] S. Ahmad and S. A. Alghamdi, "A study on effect of coarse aggregate type on concrete performance," *Arabian Journal for Science and Engineering*, vol. 37, no. 7, pp. 1777–1786, 2012.
- [12] O. Poupard, V. L'Hostis, S. Catinaud, and I. Petre-Lazar, "Corrosion damage diagnosis of a reinforced concrete beam after 40 years natural exposure in marine environment," *Cement and Concrete Research*, vol. 36, no. 3, pp. 504–520, 2006.
- [13] M. Jalal, A. Pouladkhan, O. F. Harandi, and D. Jafari, "Comparative study on effects of Class F fly ash, nano silica

- and silica fume on properties of high performance self compacting concrete,” *Construction and Building Materials*, vol. 94, pp. 90–104, 2015.
- [14] R. Yin, J. Hu, Y. Liu, Q. Wu, C. Zhang, and Y. Wang, “Study on corrosion effect of high-performance concrete under the action of sulfate and chlorine,” *International Journal of Modern Physics B*, vol. 33, 2019.
- [15] R. Heiyantuduwa, M. G. Alexander, and J. R. Mackechnie, “Performance of a penetrating corrosion inhibitor in concrete affected by carbonation-induced corrosion,” *Journal of Materials in Civil Engineering*, vol. 18, no. 6, pp. 842–850, 2006.
- [16] T. Zafeiropoulou, E. Rakanta, and G. Batis, “Performance evaluation of organic coatings against corrosion in reinforced cement mortars,” *Progress in Organic Coatings*, vol. 72, no. 1–2, pp. 175–180, 2011.
- [17] R. Anitha, S. Chitra, V. Hemapriya, I.-M. Chung, S.-H. Kim, and M. Prabakaran, “Implications of eco-addition inhibitor to mitigate corrosion in reinforced steel embedded in concrete,” *Construction and Building Materials*, vol. 213, pp. 246–256, 2019.
- [18] S. Jain and B. Pradhan, “Effect of cement type on hydration, microstructure and thermo-gravimetric behaviour of chloride admixed self-compacting concrete,” *Construction and Building Materials*, vol. 212, pp. 304–316, 2019.
- [19] A. A. Jee and B. Pradhan, “Study on development of empirical relationships between durability parameters of concrete made with different types of binder and exposed to chloride environment,” *Construction and Building Materials*, vol. 212, pp. 799–817, 2019.
- [20] Y. Wang, Y. Cao, P. Zhang et al., “Water absorption and chloride diffusivity of concrete under the coupling effect of uniaxial compressive load and freeze-thaw cycles,” *Construction and Building Materials*, vol. 209, pp. 566–576, 2019.
- [21] H. Zhang, K. Wang, X. Zhou, W. Zhu, and W. Wang, “Water quality characteristics and corrosion potential in blending zones in X city drinking water distribution system,” *Environmental Monitoring and Assessment*, vol. 190, no. 9, p. 524, 2018.
- [22] Y. Lu, C. Liu, B. Feng, X. Zhou, and L. Zhang, “Strength characteristics and mechanism analysis of high water content materials modified by silica fume,” *Bulletin of the Chinese Ceramic Society*, vol. 38, no. 9, pp. 2737–2743, 2019.
- [23] Y. Ding, G. M. Feng, and C. Z. Wang, “Experimental research on basic properties of superhigh-water packing materials,” *Journal of China Coal Society*, vol. 36, no. 7, pp. 1087–1092, 2011.